

Landslides (2017) 14:1031–1041  
 DOI 10.1007/s10346-016-0788-1  
 Received: 7 July 2016  
 Accepted: 7 December 2016  
 Published online: 13 December 2016  
 © Springer-Verlag Berlin Heidelberg 2016

Chi-Wen Chen · Hitoshi Saito · Takashi Oguchi

## Analyzing rainfall-induced mass movements in Taiwan using the soil water index

**Abstract** This study applied the soil water index (SWI), which can represent the conceptual soil water contents as influenced by present and antecedent rainfall, for analyzing rainfall-induced mass movements in Taiwan. The SWI has been used in Japan for nationwide mass movement warnings. This study examined whether the SWI can be also applied to Taiwan, which has a climatic condition and high-relief topography similar to Japan. We used data for mass movements for 2006–2012 ( $n = 263$ ) for the main analyses and those for 2013 ( $n = 19$ ) for verification. The SWI values before the rainfall events that triggered mass movements were used as the indicator of the antecedent rainfall condition. We found that when SWI values before rainfall events increased from  $<17.5$  to  $>35$ , the upper threshold of rainfall conditions needed for triggering mass movements significantly decreased. The mass movements in 2013 support this finding. We classified rainfall conditions for triggering mass movements into two types, short duration–high intensity (SH) and long duration–low intensity (LL), based on a principal component analysis (PCA). The SH type is associated with a rapid increase in SWI, and the LL type is associated with a gradual rise and subsequent constancy of SWI except in some extremely long rainfall events. Based on this result, we modeled the general trend of the time series changes in SWI for the two types, which was verified using the mass movements in 2013.

**Keywords** Landslides · Debris flows · Short duration–high intensity (SH) · Long duration–low intensity (LL) · Warning system

Rainfall-induced mass movement analysis using soil water index

### Introduction

Mass movements in mountainous areas of the world are caused mainly by three triggers: rainfall, earthquakes, and rapid snowmelt (Keefer 1984; Guzzetti et al. 2002; Malamud et al. 2004a, b; Tiranti et al. 2013) and influenced by various factors, such as topography, lithology, geological structure, soil moisture content, and anthropic influence (Crozier 1999; Glade et al. 2000; Saito et al. 2017). Numerous methodologies have been developed to detect and predict mass movement hazards. Such methodologies generally employ hydrological or statistical models to assess and map mass movement susceptibility or probability. Hydrological models assess the slope stability based on topographical, hydrological, and soil texture parameters and calculate the factor of safety along a critical slip surface using the ordinary method of slicing a landform mass or its variations (Bishop 1955; Janbu et al. 1956; Morgenstem and Price 1965; Spencer 1967; Capparelli and Tiranti 2010). In contrast, statistical models assess slope stability by analyzing site factors, such as geology, topography, climate, land use, and vegetation. Several statistical models have been used to assess mass movement susceptibility for different areas, including

logistic regression (Guzzetti et al. 1999; Dai and Lee 2002; Ayalew and Yamagishi 2005; Bui et al. 2016), artificial neural networks (Chang and Chao 2006; Lee et al. 2007; Melchiorre et al. 2008; Gorsevski et al. 2016), and decision tree models (Pal and Mather 2003; Xu et al. 2005; Bou Kheir et al. 2008; Schneevoigt et al. 2008; Saito et al. 2009; Tsangaratos and Ilia 2016). Assuming that mass movements will occur in the future due to the same conditions that triggered them in the past, susceptibility assessments predict the locations of future mass movements (Guzzetti et al. 1999, 2005, 2006; Segoni et al. 2015b; Paudel et al. 2016).

Rainfall is the most common triggering factor for mass movements. Previous studies have used rainfall characteristics, such as intensity, duration, cumulative rainfall, and antecedent rainfall during a particular period, to identify the climatological condition for mass movement initiation (Caine 1980; Keefer et al. 1987; Crozier 1999; Glade et al. 2000; Aleotti 2004; Guzzetti et al. 2007; Saito et al. 2010a; Tiranti and Rabuffetti 2010; Chen et al. 2015). Among them, the rainfall intensity ( $I$ )–duration ( $D$ ) threshold is the most popular and is applied in different areas of the world (Caine 1980; Larsen and Simon 1993; Guzzetti et al. 2007; Brunetti et al. 2010; Saito et al. 2010a; Chen et al. 2015; Rosi et al. 2016). However, the  $I$ – $D$  plot only represents average event rainfalls and does not necessarily reflect antecedent rainfall and sporadic high rainfall intensities. Previous studies also pointed out that the occurrence of mass movements is highly related to high-intensity rainfall (Saito et al. 2010a; Chen et al. 2015; Segoni et al. 2015a).

The Japan Meteorological Agency (JMA) proposed the soil water index (SWI) as the conceptual soil water contents influenced by present and antecedent rainfall (Okada et al. 2001). This index uses a calculated value of the total water depth of a three-layer tank model with fixed parameters (Sugawara et al. 1974; Ishihara and Kobatake 1979). Using the SWI, the Japanese government established a nationwide early warning system for mass movement disasters in 2005. The system sets a criterion for the occurrence of mass movements based on a 60-min cumulative rainfall and the SWI in each 5-km grid cell covering all areas of Japan (Osanaï et al. 2010).

Saito et al. (2010b) proposed the normalized soil water index (NSWI), which is the SWI divided by the highest value of the SWI over the past decade. They identified two types of rainfall conditions for shallow landslide initiations in Japan: a short-duration–high-intensity (SH) type and a long-duration–low-intensity (LL) type. This classification can be used for predicting shallow landslides resulting from the rapid increase in the NSWI with short duration (SH) and those from the gentle rise in the NSWI followed by heavy rainfalls of long duration (LL). The NSWI was then used for a regional case study of landslide disasters triggered by a record-breaking rainfall due to Typhoon Talas in September 2011 that caused enormous damage in the Kii Peninsula, Japan. Most of the landslides occurred in an area where the maximum NSWI was high (Saito and Matsuyama 2012).

In Japan, the SWI was also used to assess the influence of antecedent rainfall (Sassa 2005). For example, the investigation team for landslide disasters triggered by the Mid-Niigata Prefecture earthquake in 2004 used the SWI to analyze the influence of rainfall before the earthquake (Sassa 2005). The heavy rainfall prior to the Mid-Niigata Prefecture earthquake resulted in numerous landslides and significantly differed from the results in the Nikawa landslide caused by the Hyogoken-Nambu earthquake in 2005 with a long travel distance and almost no antecedent rainfall. These previous studies show that the SWI can successfully predict the occurrence of mass movements, but it has been verified only in Japan.

Since mass movements are densely and widely distributed in Taiwan, it is important to establish the relationship between the initiation of mass movements and the rainfall conditions. In order to combine the effects of antecedent and current rainfall intensities and contribute to mass movement warnings, it seems appropriate to apply the SWI to Taiwan. Both Taiwan and Japan are located on the ring of fire where active orogeny resulted in many high mountains higher than 3000 m a.s.l. The highest peaks in Taiwan and Japan are 3952 m of Yushan and 3776 m of Mount Fuji, respectively. Previous studies also show that the slope of around 30° is the most relevant with mass movements in Taiwan (Chen et al. 2015, 2016) and in Japan (Fujiwara et al. 2004). In terms of climate, Taiwan and Japan mostly belong to the climate of the temperate zones and under the influence of the Asian monsoon. The annual rainfall in Taiwan and Japan average 2500 and 1700 mm, respectively, and on average, three to four typhoons strike both areas every year. Figure 1 shows simplified geological maps of Taiwan and Japan based on the 1:500,000 Taiwan Geological Map from the Central Geological Survey of Taiwan and the 1:200,000 Japan Seamless Geological Map from the Geological Survey of Japan. Geological conditions in both Taiwan and Japan are those of island arc formed under strong tectonic stresses. Such topographic, climatic, and geologic similarities between Taiwan and Japan suggest the applicability of the SWI in both areas. Although other factors, such as vegetation and soil types, also affect the occurrence of mass movements, the SWI offers a straightforward means for issuing mass movement warnings for a wide area. Therefore, the objective of this study is to examine the applicability of the SWI in Taiwan to analyze the relationship between mass movements and rainfall conditions.

### Study area

Taiwan is located on a convergent plate boundary between the Eurasian Continental and the Philippine Sea plates, with the latter subducting below the former at a rate of 80 mm/year (Yu et al. 1997). The subduction resulted in the formation of an active mountain belt called the Central Range with over 200 peaks higher than 3000 m a.s.l. (Ho 1986; Teng 1990). It is also responsible for frequent large earthquakes and an orogenic uplift rate of about 5 to 7 mm/year (Li 1976; Willett et al. 2003). About 32% of Taiwan is above 1000 m a.s.l. The slope of the mountainous areas is mostly between 30° and 50° (Chen et al. 2015) with a dominance of 35° (Lin et al. 2009).

Taiwan is located between 120° E and 122° E and between 22° N and 25° N, and the boundary between tropical and subtropical

monsoon climates is located in the south of Taiwan (Wang and Ho 2002). The average temperature over the Taiwanese lowlands during the wet season (May to October) is above 20 °C, while that during the dry season (November to April), it is between 14 and 20 °C. On average, four typhoons strike Taiwan every year (Wu and Kuo 1999), causing heavy and concentrated rainfall. The annual rainfall in Taiwan averages 2500 mm. However, the annual rainfall in the mountainous regions can surpass 3000 mm (Shieh 2000). Approximately 60 to 80% of the rainfall occurs during the wet season (Chen et al. 2015).

Mass movements, particularly landslides and debris flows, are triggered by frequent rainfall and earthquakes, which represent the primary mechanisms of erosion and are important for maintaining the balance between erosion and uplift in Taiwan (Dadson et al. 2003). Taiwan also has a fragile geological environment, with areas of geological discontinuity that are more prone to mass movements (Chen et al. 1999; Chen and Su 2001; Chuang et al. 2009).

### Data and methods

#### Mass movement data

This study analyzed 263 mass movements caused by heavy rainfall during the 7-year period between 2006 and 2012 and used 19 mass movements that occurred in 2013 for verifying the results (Fig. 2). These mass movements occurred in various places in Taiwan during the wet season: two in May, 26 in June, 35 in July, 152 in August, 27 in September, and 40 in October (Fig. 3).

We collected mass movement data from the reports of the Soil and Water Conservation Bureau (SWCB) of Taiwan. The SWCB has conducted detailed field surveys when rainfall-induced mass movement disasters, such as damage to houses and roads, occurred to prevent secondary disasters and allow for a quick recovery. The resultant reports contain information on the type, location, and approximate time (accuracy in hours) of each disaster event. They estimate the time based on real-time videos taken at observation stations, the time when people reported the disasters, and interviews with residents. They investigate the extent of the affected areas and the damage to residences and buildings. The disasters in these reports are classified into three types: landslides, debris flows (mostly channelized debris flows and some slope debris flows), and floods. We selected landslides and debris flows for our analysis. The landslides may include falls or topples related to gravity alone. Therefore, we carefully checked all reports (314 mass movements) and excluded 32 mass movements with almost no rainfall during the mass movements.

#### Rainfall data

Since 2012, the Central Weather Bureau (CWB) and the Water Resource Agency (WRA) of Taiwan developed the Quantitative Precipitation Estimation and Segregation Using Multiple Sensors (QPESUMS), a radar system, to estimate rainfall depth and its spatial distribution (Chen et al. 2007; Chiang and Chang 2009). However, the radar system in Taiwan is unstable and the data contain many uncertainties. For Taiwanese researchers, the most commonly used rainfall data are still those from rain gauges (Chen 2016; Chou et al. 2016) and their interpolated values (Tao et al. 2009). The CWB has installed more than 400 rain gauges with a

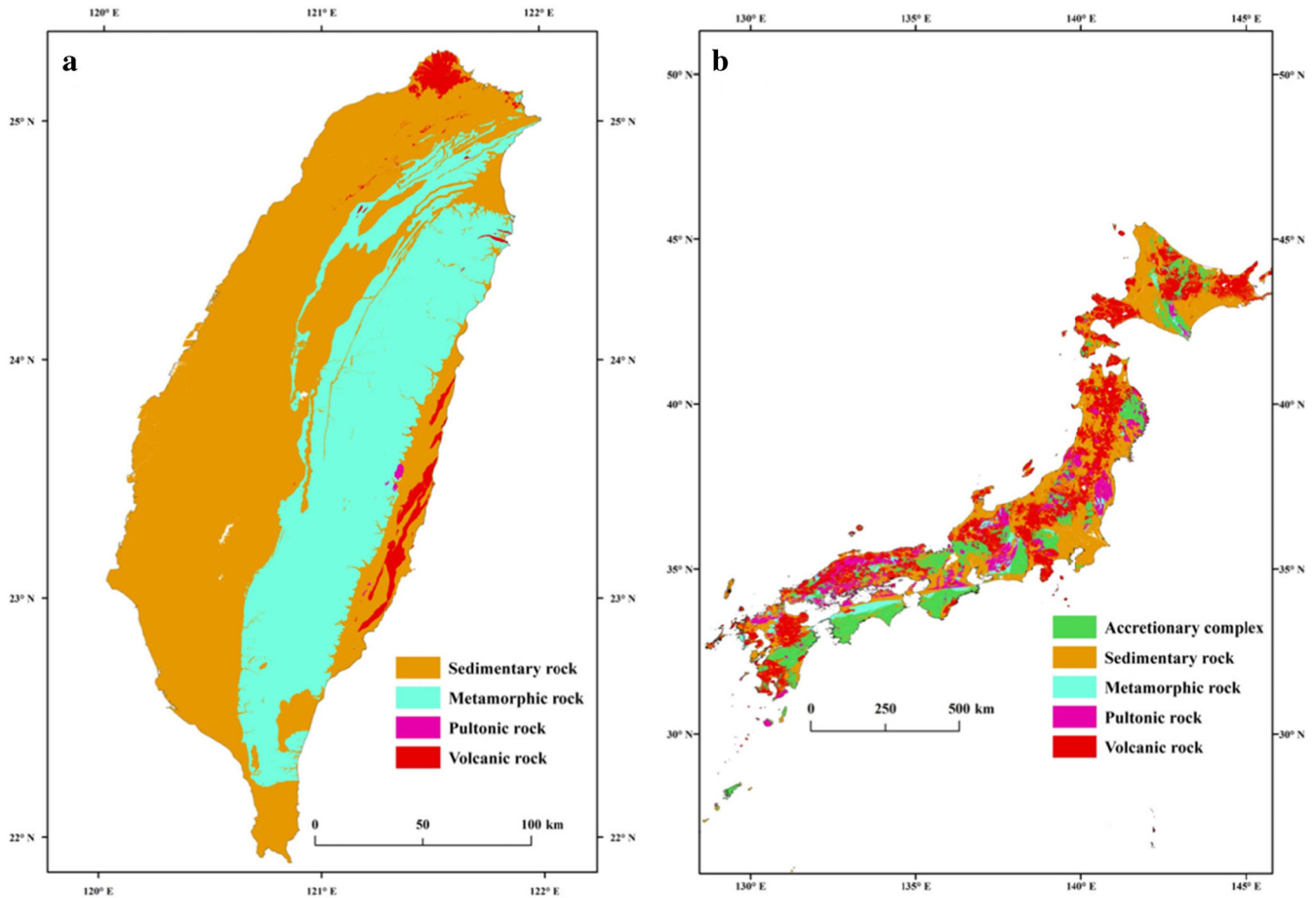


**Fig. 1** Geological maps of a Taiwan and b Japan, simplified after the 1:500,000 Taiwan Geological Map from the Central Geological Survey of Taiwan and the 1:200,000 Japan Seamless Geological Map from the Geological Survey of Japan

density of approximately one gauge for every 76 km<sup>2</sup> (Fig. 2) that record hourly data. These rain gauges are the tilting-bucket type, which can be used for automated observations. Since rain gauges were not always located close to the mass movement sites and relatively few rain gauges were distributed in the mountainous areas, we usually selected the nearest five rain gauges within 10 km from each mass movement to estimate rainfall at each mass movement location. The selected rain gauges are on the same side of the hillslope as the mass movements, avoiding the mountain effect. If five rain gauges based on this principle did not exist, we then only selected available rain gauges. If the number of available rain gauges is less than three, we then selected the data from the nearest rain gauge without interpolation. This included conducting a kriging interpolation using the ordinary kriging and the spherical semivariogram model with a variable search radius. We obtained the hourly rainfall value at the location of each mass movement in this manner. Although the commonly used definition of one rainfall event in Taiwan is considered to begin when hourly rainfall surpasses 4 mm and ends when hourly rainfall decreases below 4 mm over the next six consecutive hours (Jan and Lee 2004; Chen et al. 2015), we did not use a peak-over-threshold approach to identify individual events to compute uncensored rainfall totals. Many previous studies have proposed

different non-rainfall intervals for defining one rainfall event (Tiranti and Rabuffetti 2010; Vessia et al. 2014; Melillo et al. 2015). From them, we chose one continuous rainfall event as the rainfall period delimited by a non-rainfall period of more than 24 h, which is most commonly used in Japan (Osanai et al. 2010; Saito et al. 2010a, b, 2014).

For verifying the relationship between the mass movements and rainfall using the SWI, the conditions of the rainfall events corresponding to the individual mass movements are needed. Therefore, we also calculated the mean rainfall intensity ( $I$ , mm/h), rainfall duration ( $D$ , h), and cumulative rainfall (mm) from the beginning of a rainfall event to the time of the mass movement occurrence. We used the mean rainfall intensity because it is used for the most popular rainfall threshold ( $I$ - $D$  threshold) established by many previous studies.

#### Soil water index

The SWI uses a calculated value of the total water depth of a three-layer tank model with fixed parameters (Sugawara et al. 1974; Ishihara and Kobatake 1979) (Fig. 4). Previous studies in Japan used the SWI for assessing and predicting potential mass movements (Okada et al. 2001; Sassa 2005; Osanai et al. 2010;

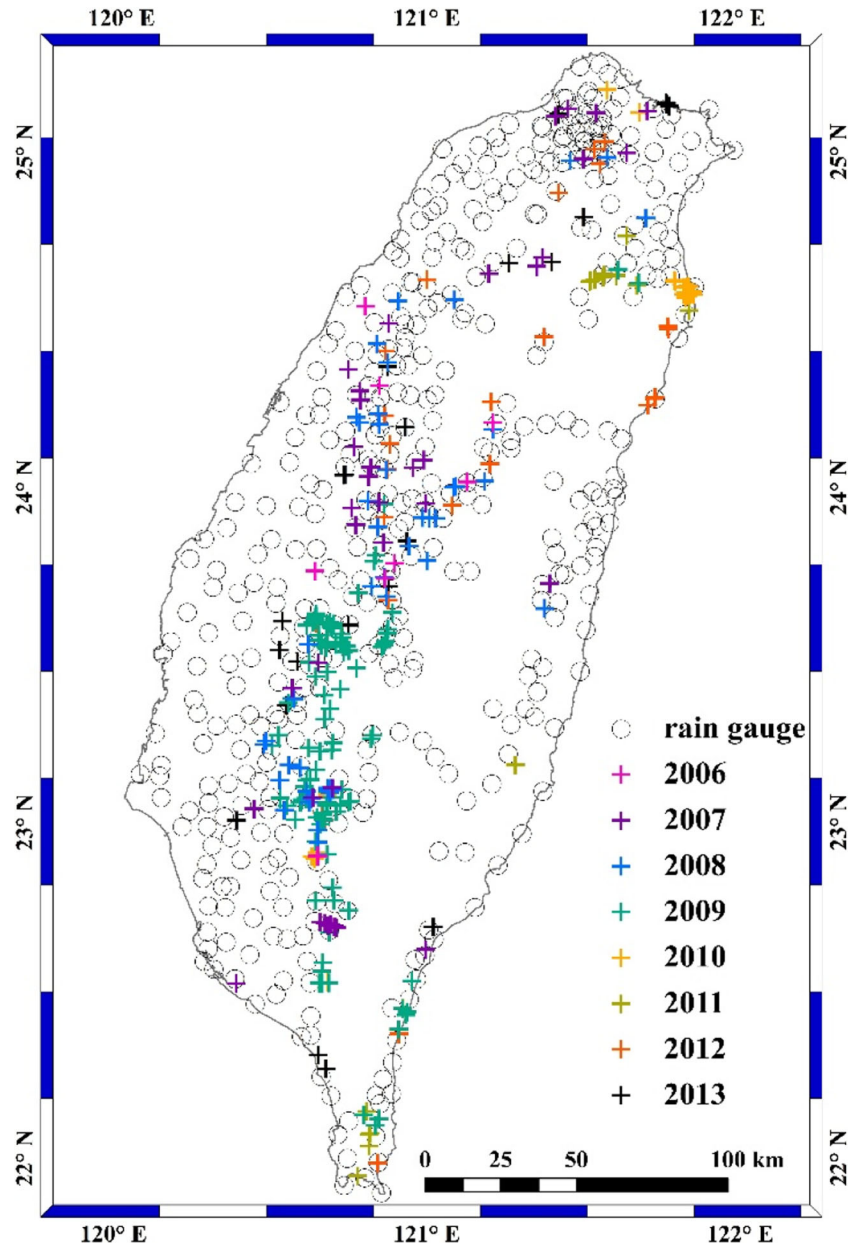


**Fig. 2** Distribution of rain gauges and mass movements that occurred between 2006 and 2013

Saito et al. 2010b; Saito and Matsuyama 2012; Oku et al. 2014) and also for establishing early warning systems for mass movements (Osanaï et al. 2010). The heavy rainfall increases soil moisture contents, which increases the possibility of mass movements. The tank model is a hydrological model to calculate the water discharge and amount in the near-surface soil layers and estimate the total amount of rainwater in soil from the rainfall data. The formula for SWI is as follows :

$$SWI(t + \Delta t) = \sum_k S_k(t + \Delta t) \quad (1)$$

where  $t$  is the time (h);  $\Delta t$  is the passed time (h, calculated per hour according to the resolution of rainfall data);  $k = 1, 2,$  and  $3$  indicate the top, middle, and bottom tanks, respectively; and  $S_k$  is

the remaining water height (mm) for each tank, which can be calculated as follows:

$$S_k(t + \Delta t) = \begin{cases} S_k(t) - \left[ \sum_l Q_{kl}(t) + Z_k(t) \right] + R(\Delta t) & (k = 1) \\ S_k(t) - \left[ \sum_l Q_{kl}(t) + Z_k(t) \right] + [Z_{k-1}(t + \Delta t) - Z_{k-1}(t)] & (k \geq 2) \end{cases} \quad (2)$$

where  $Q_{kl}$  is the outflow volume from the  $l$ th side hole (the first tank has two holes on the side and the other tanks have one),  $Z_k$  is the vertical permeation volume from the bottom of the  $k$ th tank,



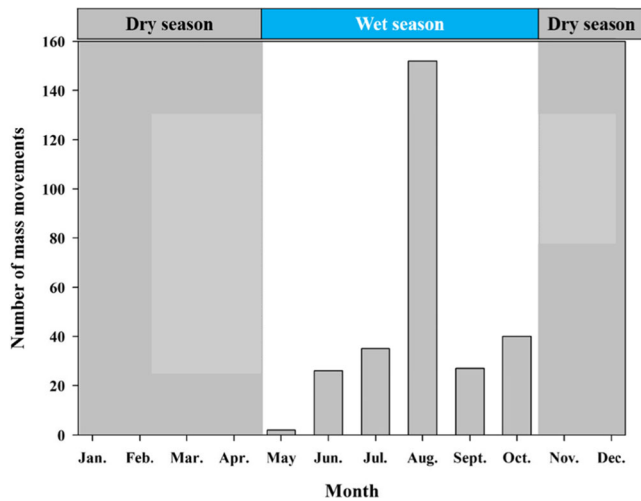


**Fig. 3** Number of the collected mass movements for each month with the wet season from May to October and the dry season from November to April

and  $R(\Delta t)$  is the 1-h rainfall amount.  $Q_{kl}$  and  $Z_k$  at  $t$  are calculated as follows:

$$Q_{kl}(t) = \begin{cases} \alpha_{kl}\{S_k(t) - L_{kl}\} & (S_k(t) > L_{kl}) \\ 0 & (S_k(t) \leq L_{kl}) \end{cases} \quad (3)$$

$$Z_k(t) = \beta_k S_k(t) \quad (4)$$

where  $\alpha_{kl}$  is the outflow coefficient (1/h) for the  $l$ th side hole,  $\beta_k$  is the coefficient of permeability (1/h) from the bottom hole of the  $k$ th tank, and  $L_{kl}$  represents the outflow height (mm) on the  $l$ th side hole of the  $k$ th tank.

The Japanese government set different reference values for each 1-km<sup>2</sup> area to provide a warning when the heavy rainfall comes and the SWI exceeds the reference value ([http://www.jma.go.jp/jma/kishou/known/kijun/index\\_shisu.html](http://www.jma.go.jp/jma/kishou/known/kijun/index_shisu.html)). The fixed parameters ( $\alpha_{kl}$ ,  $\beta_k$ , and  $L_{kl}$ ) were identified by the statistical analysis of the relationship between rainfall and discharge in Japan (Sugawara et al. 1974; Ishihara and Kobatake 1979) as shown in Table 1. Although both Japan and Taiwan are characterized by complex geological conditions, the SWI only represents the conceptual soil water contents, and the time series change in SWI exhibits a similar trend when the parameters are adjusted to different areas. Therefore, the Japanese government applies the SWI to the whole of Japan using the fixed parameters in spite of various geological conditions. For this reason, this study applies the SWI to Taiwan using the fixed parameters. The values of SWI were calculated over 1 month before the occurrence time of each mass movement to see the effect of antecedent rainfall (Fig. 5).

#### Classification of rainfall conditions and establishing the general trends of the SWI

We grouped the 263 mass movements during 2006–2012 into the SH and LL types and then validated the result by analyzing 19 mass movements from 2013.

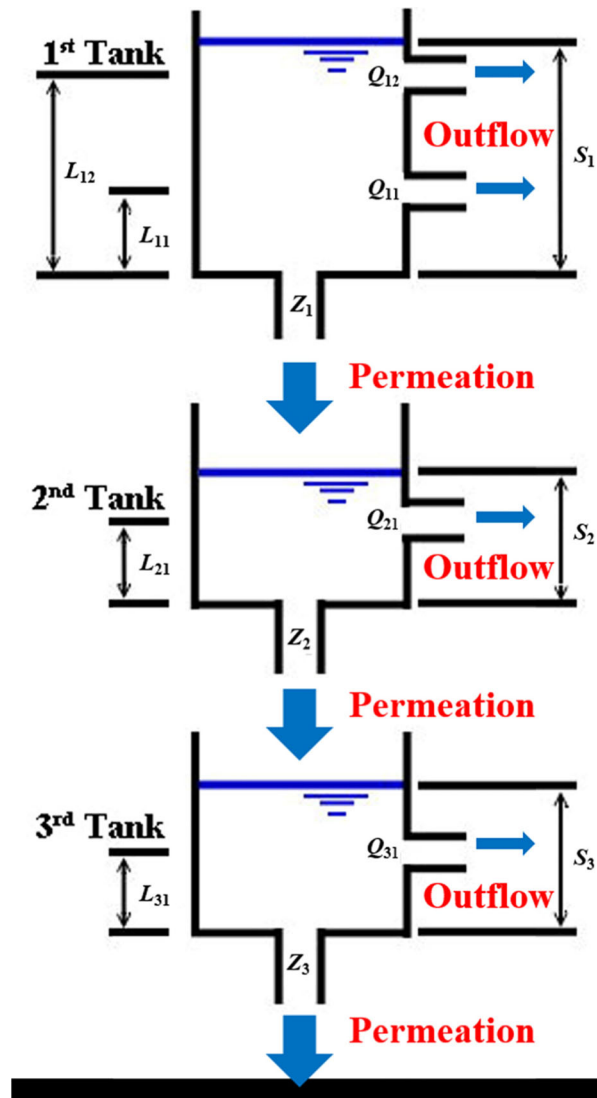


**Fig. 4** Schematic diagram of the three-layer tank model. The SWI is a calculated value of the total water depth in each layer (Okada et al. 2001); parameters of each layer are shown in Table 1

Saito et al. (2010b) pointed out that changes in the NSWI of the SH and LL types from the beginning of rainfalls to mass movement occurrence show different trends. The non-parametric median regressions can determine the general trend of the NSWI for the two rainfall types (Saito et al. 2010b). We also adopted this procedure for Taiwan to establish the general trends of the two rainfall types but used the SWI instead of the NSWI. Because the most common rainfall data in Taiwan are from rain gauges, the hourly rainfall data for at least 10 years should be collected and interpolated for calculating the NSWI. In addition, Taiwan is a relatively small district where the regional difference in the highest value of SWI is expected to be smaller than in Japan. For these reasons, we adopted the SWI for Taiwan.

#### Results and discussion

##### Rainfall conditions and the SWI for mass movements

The PCA was adopted to classify the  $I$ - $D$  conditions of mass movement events during 2006–2012 (Fig. 6). Two types of  $I$ - $D$

**Table 1** Parameters for the SWI

Tank	First	Second	Third
Outflow height (mm)	$L_{11} = 15$ $L_{12} = 60$	$L_{21} = 15$	$L_{31} = 15$
Outflow coefficient (1/h)	$\alpha_{11} = 0.1$ $\alpha_{12} = 0.15$	$\alpha_{21} = 0.05$	$\alpha_{31} = 0.01$
Coefficient of permeability (1/h)	$\beta_1 = 0.12$	$\beta_2 = 0.05$	$\beta_3 = 0.01$

conditions are distributed along with the two PCs. The proportion of variance along with the positives and negatives of the first PC was 71.8% and that for the second PC was 28.2%. The positives of the first PC score (120 mass movement events) mainly occur when rainfall persists for 29–77 h from the beginning of the rainfall event (53 h on average with 24 h of standard deviation), which represent SH rainfalls. Conversely, the negatives (143 mass movement events) mainly occur when rainfall persists for 80–170 h (125 h on average with 45 h of standard deviation), which represent LL rainfalls. In Fig. 6, we also plotted the rainfall conditions of the 19 mass movements that occurred in 2013. The rainfall conditions were classified into 14 SH types and five LL types.

During 2006–2012, the changes in the SWI show that the SWI before a rainfall event was 17.5 on average, ranging from 0.0 to 105.0. The SWI for the time of the mass movement occurrences was 336.8 on average, ranging from 68.6 to 645.0. The differences were 319.3 on average, ranging from 47.8 to 639.1. Table 2 shows that the SWI results for the SH and LL types are not much different for both before rainfall and when mass movement occurred. In 2013, the SWI before the rainfall events was 36.0 on average, ranging from 3.8 to 91.9. The SWI for the time of mass movement occurrences was 154.4 on average, ranging from 81.7 to 220.7. The differences were 118.4 on average, ranging from –10.2 to 213.4. All values of the SWI in 2013,

except for those before a rainfall event, were smaller than those during 2006–2012. Figure 6 also shows that the rainfall conditions in 2013 tend to be lower on the  $I$ - $D$  plot than in the other years. Overall, the SWI changed dramatically from the beginning of the rainfall to the mass movement occurrence, and the rapid increase in the SWI resulted in the mass movements. Figure 5 shows an example of time series changes in the SWI from 1 month before the mass movements. Before the mass movements occurred, the SWI oscillated several times with precipitation. The rainfall then elevated the SWI to its highest value, resulting in a mass movement. Data for the other rainfall events also show that mass movements occurred around the peaks in the SWI because the maximum soil water content causes the most significant decrease in resistant strength and increase in the sliding force of slopes. This observation shows that changes in SWI and high SWI values are closely related to mass movement occurrence.

The 263 mass movements during 2006–2012 can be separated into three groups by two values of SWI before a rainfall event, 17.5 (the average value) and 35 (twice the average value), respectively. Table 3 shows the 98th percentile of mean intensity, duration, and cumulative rainfall for these three groups. We used the 98th percentile because of its resistance to outliers. The 98th percentile of rainfall conditions for  $SWI \geq 35$  is 25.8 mm/h in mean intensity, 105 h in duration, and 1159.8 mm in cumulative rainfall. Those for  $17.5 < SWI < 35$  are 23.9 mm/h, 189 h, and 1403.4 mm, and those for  $SWI \leq 17.5$  are 24.1 mm/h, 225 h, and 1745.9 mm (Fig. 7). The number of data for the group  $SWI \geq 35$  is relatively small, and two cases in this group with relatively high intensity led to the high 98th percentile mean intensity.

#### Hourly changes of SWI for the SH and LL rainfall types

As mentioned in the previous section, a rainfall event that elevates SWI to a high value is important for the occurrence of mass movement. Therefore, identifying changes in SWI helps in understanding mass movements. Figure 8 shows the hourly changes in SWI for the SH and LL rainfall types from the beginning of the

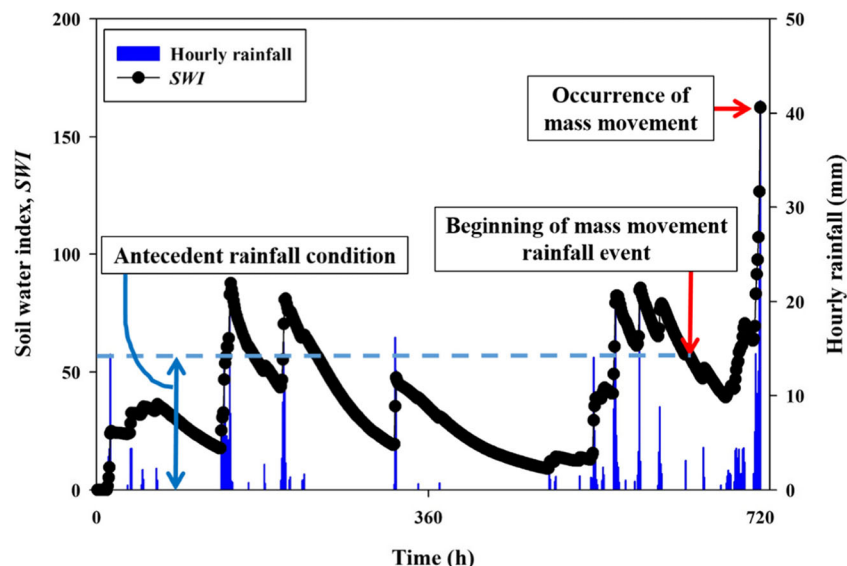


**Fig. 5** Example of change in the SWI; the vertical red arrow shows the beginning of the rainfall event that caused a mass movement; the horizontal red arrow shows the occurrence of the mass movement; the blue arrow and the dashed line show the SWI before the rainfall event representing the antecedent rainfall condition

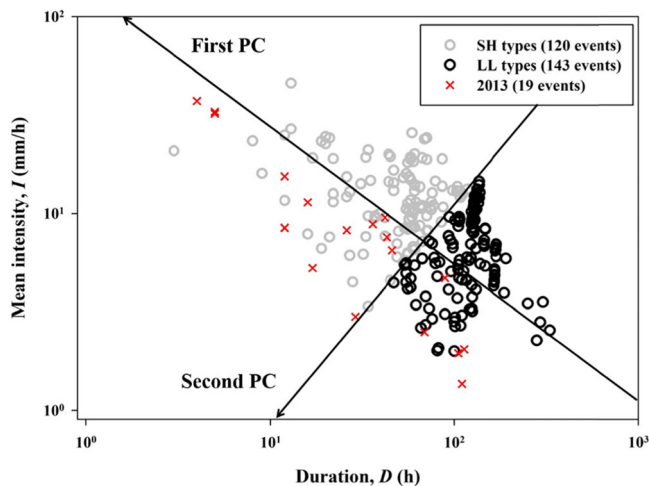


**Fig. 6** PCA for  $I-D$  conditions of mass movements; gray circles and black circles are SH and LL types, respectively, and red crosses are data for 2013

rainfall events to mass movement occurrences, based on the data for the years 2006–2012. Non-parametric median regressions were adopted to determine the general trends of the SWI of these two types shown in Fig. 8.

The SH type shows that the SWI rises rapidly within a duration of 100 h and exceeded 150 for more than 90% of the events. This result shows that a rapid increase in soil water contents with a short duration is responsible for mass movement initiation in the SH type. The SWI of the LL type gently rises to about 150 and tends to have a peak at 130 h. After 130 h, the SWI decreases slightly and then goes up again after 250 h. Although the LL curve is not located at the high domain where mass movements are initiated, the temporal change in the SWI for each event is large. Many events were associated with high SWI values, which reveal that sporadic high-intensity rainfall also occurs during long-term rainfall. This raises soil water contents and causes mass movements. Therefore, a gentle rise in the SWI over a long duration from the beginning of a rainfall event, followed by heavy rainfall, is critical for mass movement initiation for the LL type.

### Verification of inferences from the SWI

The observations in the previous sections based on data for 2006–2012 were tested by analyzing 19 rainfall-induced mass movements from 2013. The SWI values before rainfall events and rainfall conditions of mass movements are shown in Fig. 9. Most of them correspond to the rainfall conditions of 2006–2012, confirming that the SWI can be used as an indicator of antecedent conditions and for detecting the upper threshold of rainfall conditions for mass movements. However, there are still several cases that exceeded the upper threshold: three cases for rainfall intensity and two cases for rainfall duration. Even so, the exceeded values are very close to the upper threshold except the three cases when the rainfall intensities are as high as 37.3, 32.9, and 32.2 mm/h, while the SWI before the rainfall event is between 17.5 and 35.

The rainfall conditions of the 19 mass movements were classified into 14 SH types and five LL types (Fig. 6). The changes in the SWI of the mass movements in 2013 also followed the trends of the predefined SH and LL curves (Fig. 10). The cases of the SH type generally followed the SH general curve from the beginning of

**Table 2** Changes in the SWI during 2006–2012 and in 2013

Moment	SWI (2006–2012) Before rainfall		Mass movement		Difference		SWI (2013) Before rainfall	Mass movement		Difference	
	SH	LL	SH	LL	SH	LL		SH	LL	SH	LL
Average	18.8	16.4	314.5	355.5	295.7	339.1	28.8	165.1	124.3	136.3	68.3
Max.	85.9	105.0	563.2	645.0	545.3	639.1	61.6	220.7	180.8	213.4	125.5
Min.	0.0	0.0	68.6	146.2	61.7	47.8	3.8	87.3	81.7	61.5	-10.2

**Table 3** The 98th percentile of mean intensity, duration, and cumulative rainfall of mass movements in different ranges of SWI before rainfall events

Rainfall conditions	SWI $\leq 17.5$ ( $n = 167$ )	$17.5 < \text{SWI} < 35$ ( $n = 75$ )	SWI $\geq 35$ ( $n = 21$ )
Mean intensity (mm/h)	24.1	23.9	25.8
Duration (h)	225	189	105
Cumulative rainfall (mm)	1745.9	1403.4	1159.8

rainfall but then rose from the SH general curve, resulting in mass movements. In contrast, the LL types were vaguely located between the SH and LL general curves at the early stage. They started to follow the LL general curve about 30–40 h after the beginning of rainfall and continued until the occurrence of mass movements. There is one exceptional case in the LL type. Its SWI value once followed the SH curve and rapidly increased, but mass movements did not happen at that time. Instead, mass movements occurred after the SWI decreased and followed the LL curve. The hourly rainfall for this case was less than 5 mm until 37 h after the beginning of the rainfall event. Suddenly, high-intensity rainfall (about 32 mm/h) occurred during 38–45 h, but after that, rainfall stopped for a long period. The next intense rainfall occurred 38 h after the rainfall had stopped. This means that the first high-intensity rainfall increased the SWI rapidly and the slope became unstable. However, since the rainfall suddenly stopped, the mass movements did not occur at that time. Soon after the next intense rainfall, mass movements occurred.

The verification confirmed the advantages of using the SWI. For example, the SWI of the LL type often increased rapidly before mass movements (Fig. 8), which can be used for warnings. This phenomenon cannot be found in the  $I$ - $D$  threshold, because the  $I$ - $D$  plot represents average event rainfall and does not necessarily reflect sporadic high rainfall intensities. This study established the general curves of changes in SWI for the SH and LL types that can be used to determine whether a rainfall event belongs to the SH or LL type during rainfall monitoring and to evaluate the likelihood of mass movements. Therefore, the combined use of the  $I$ - $D$  threshold and SWI is recommended to local authorities for making appropriate decisions in preventing mass movement hazards.

#### Significance of the SWI for worldwide mass movement warnings

The SWI represents conceptual soil water contents in the near-surface soil layers that can be easily calculated using the tank model based on rainfall analysis (Fig. 5). Unlike many other hydrological models that require a significant amount of data, such as surface materials, soil thickness, and sliding surface features of each slope, the SWI provides a simplified model using only rainfall with fixed parameters to allow application to wide areas.

Our results indicate that with the increase in the SWI, the rainfall conditions needed for triggering mass movements, such as duration and cumulative rainfall, decrease (Fig. 7). To determine the lower threshold of rainfall conditions for mass movements is often difficult because some areas experience mass movements frequently due to topographic and geological conditions even if the impact of rainfall is relatively small (Chen et al. 2015). However, even from the upper threshold and the SWI, we can also know that the present rainfall conditions needed for

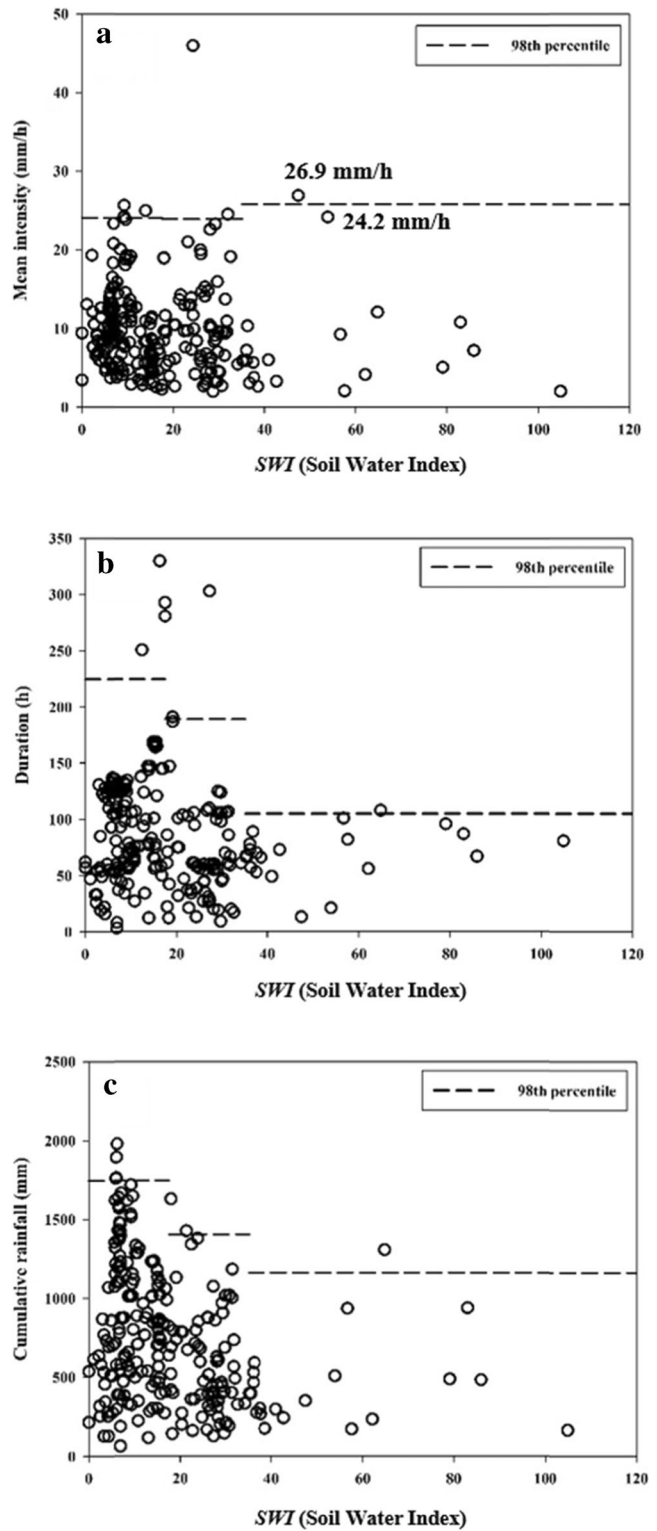


**Fig. 7** Comparing the SWI before rainfall events with the rainfall conditions of a mean intensity, b duration, and c cumulative amount during 2006–2012; indicated values are two cases with high intensity in the group SWI  $> 35$ ; dashed lines represent the upper thresholds of rainfall conditions in different ranges of SWI

triggering mass movements decrease due to the antecedent rainfall. This means that the SWI can be used as an indicator for



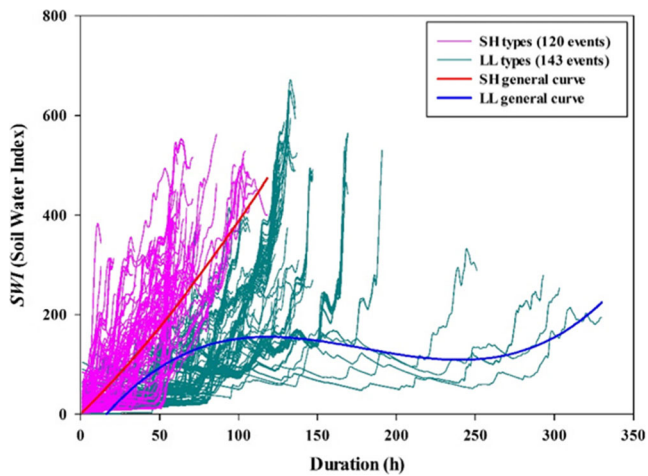


**Fig. 8** Hourly changes in the SWI from the beginning of rainfall events to mass movement occurrence between the two types of rainfall condition during 2006–2012

assessing the effect of antecedent rainfall on mass movements and is better than using only the total amount of antecedent rainfall. Actually, there are many different definitions for antecedent rainfall in terms of its length, such as 3 days (Kim et al. 1991); 4 days (Heyerdahl et al. 2003); and 7, 10, 15, and 30 days (Crozier 1999; Glade et al. 2000; Aleotti 2004; Dahal and Hasegawa 2008; Khan et al. 2012; Chen et al. 2015). To date, it is still difficult to determine the appropriate length of antecedent rainfall, and using the SWI solves this problem. The SWI is calculated based on the permeation and outflow of water by a three-layer tank model that continuously reflects soil water contents. Unlike models using only rainfall, effects of antecedent rainfall can be reflected.

This study also combined the SWI with statistical methods to identify general curves for the changes in the SWI between the beginning of a rainfall event and mass movement occurrence (Fig. 8). These general curves can be used as references to judge the possibility of mass movements similar to previously proposed statistical methods that establish a threshold for mass movements, such as the  $I$ - $D$  threshold. Although the  $I$ - $D$  threshold can be used for a wide area, it only represents average event rainfalls and does not necessarily reflect sporadic high rainfall intensities, although mass movements tend to occur in such conditions (Chen et al. 2015). The SWI before a rainfall event that caused a mass movement reflects the influence of antecedent rainfall, and the rapid increase in the SWI reflects a sporadic intense rainfall. A rapid increase in SWI combined with high SWI values leads to mass movements (Fig. 10), indicating that SWI more exactly predicts the time of mass movement occurrence. In addition, for an extremely long rainfall event (>200 h), when rainfall becomes slightly weak, the SWI may decrease as the rate of runoff is faster than infiltration. However, if there is a sudden heavy rainfall, the SWI rapidly increases and mass movements still occur (Fig. 8). Therefore, in such extremely long rainfall events, continuous and careful observation of the change in the SWI is necessary.

Although the mechanisms of rainfall-induced mass movements may be various, they are generally due to gradual increases in groundwater level, soil moisture, and pore water pressure that cause slope instability (Wieczorek and Glade 2005). Therefore, the SWI seems to be applicable to various

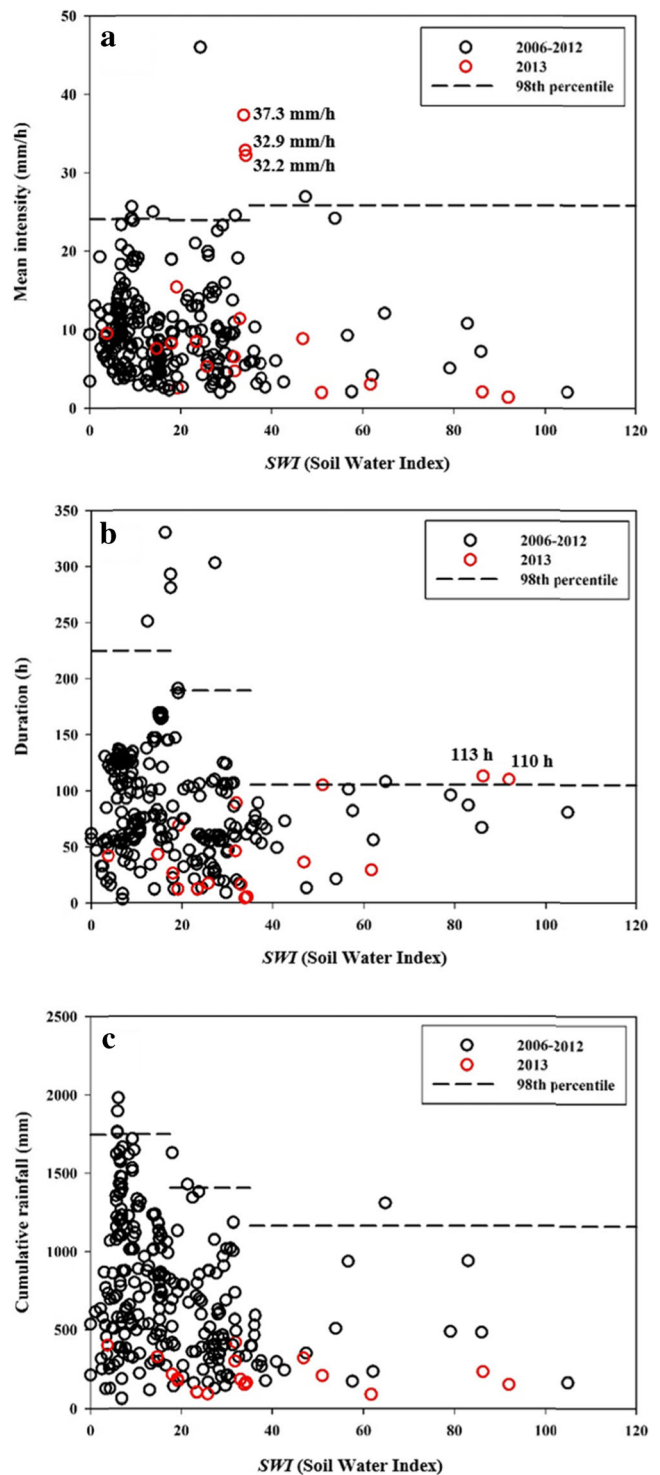


**Fig. 9** Verification of the SWI analysis using data for 2013: **a** mean intensity, **b** duration, and **c** cumulative rainfall; *dashed lines* represent the upper thresholds of rainfall conditions in different ranges of SWI; indicated values are the cases exceeding the upper thresholds in 2013

areas other than Japan and Taiwan. However, Japan and Taiwan have similar climatic conditions and high-relief topography. Future research needs to test the SWI in areas with other climatic and topographic conditions.

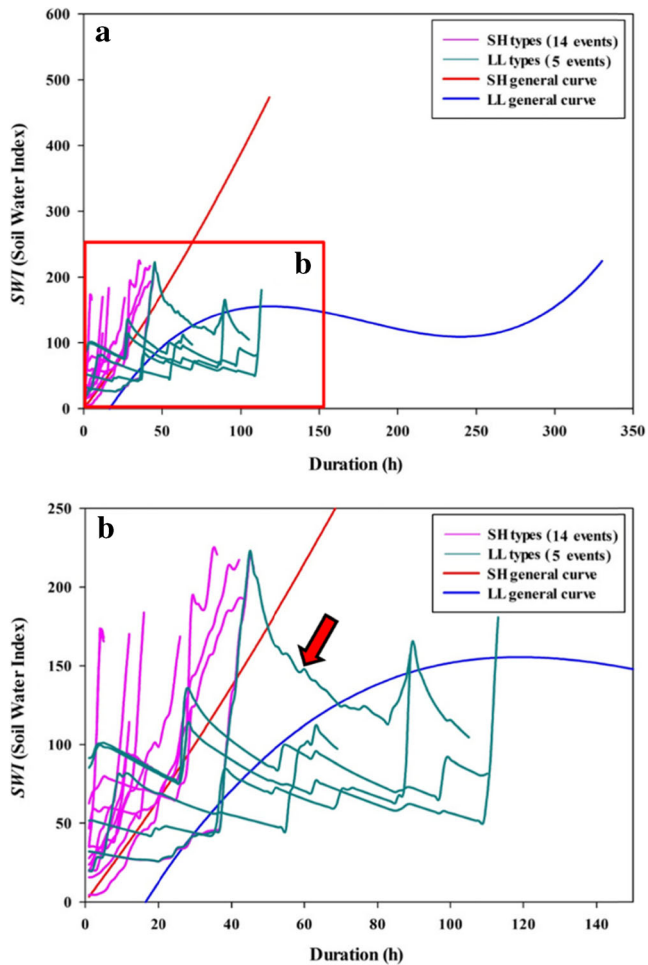


**Fig. 10** Verification of the changing trends in the SWI for the two types of rainfall conditions using data for 2013; the *red arrow* shows the exceptional case of the LL type in 2013

### Conclusions

The SWI has been used by the JMA to assess mass movement hazards in Japan. This study in Taiwan has applied the SWI to an area other than Japan for the first time. For different values of SWI before rainfall events, the rainfall conditions needed for triggering mass movements, such as the rainfall duration and cumulative amount, are different. When higher values of SWI are observed before rainfall events, the upper threshold of rainfall conditions needed for triggering mass movements will be lower. Therefore, the SWI can be used as the indicator of the antecedent rainfall condition. We classified the rainfall condition into two types, SH and LL, based on a PCA. The two types performed differently with changes in the SWI. The SH type is associated with a rapid increase in SWI within a short duration, and the LL type is associated with a gradual rise and subsequent constancy of SWI except in some extremely long rainfall events. Therefore, a rapid increase in soil water during a short duration is responsible for mass movements in the SH type, while the gentle increase in soil water over a long duration, followed by heavy rainfall, is critical for mass movements in the LL type. The observations were verified by analyzing 19 mass movements that

occurred in 2013. We recommend the use of the SWI to establish a suitable warning system for mass movements in Taiwan.

### Acknowledgements

We would like to thank the Typhoon and Flood Research Institute (TTFRI) of Taiwan for providing rainfall data and the Soil and Water Conservation Bureau (SWCB) of Taiwan for providing information on mass movements. This work was supported by the Japan Society for the Promotion of Science (JSPS) KAKENHI Grant Number 15K12452.

### References

- Aleotti P (2004) A warning system for rainfall-induced shallow failures. *Eng Geol* 73:247–265
- Ayalew L, Yamagishi H (2005) The application of GIS-based logistic regression for landslide susceptibility mapping in the Kakuda–Yahiko Mountains, Central Japan. *Geomorphology* 65:15–31
- Bishop AW (1955) The use of the slip circle in the stability analysis of slopes. *Geotechnique* 5:7–17
- Bou Kheir R, Chorowicz J, Abdallah C, Dhont D (2008) Soil and bedrock distribution estimated from gully form and frequency: a GIS-based decision-tree model for Lebanon. *Geomorphology* 93:482–492
- Brunetti MT, Peruccacci S, Rossi M, Luciani S, Valigi D, Guzzetti F (2010) Rainfall thresholds for the possible occurrence of landslides in Italy. *Nat Hazard Earth Sys* 10:447–458
- Bui DT, Tuan TA, Klempe H, Pradhan B, Revhaug I (2016) Spatial prediction models for shallow landslide hazards: a comparative assessment of the efficacy of support vector machines, artificial neural networks, kernel logistic regression, and logistic model tree. *Landslides* 13:361–378
- Caine N (1980) The rainfall intensity–duration control of shallow landslides and debris flows. *Geogr Ann A* 62:23–27
- Capparelli G, Tiranti D (2010) Application of the MoniFLaR early warning system for rainfall-induced landslides in Piedmont region (Italy). *Landslides* 7:401–410
- Chang TC, Chao RJ (2006) Application of back-propagation networks in debris flow prediction. *Eng Geol* 85:270–280
- Chen CY (2016) Landslide and debris flow initiated characteristics after typhoon Morakot in Taiwan. *Landslides* 13:153–164
- Chen H, Su DI (2001) Geological factors for hazardous debris flow in Hoser, Central Taiwan. *Environ Geol* 40:1114–1124
- Chen H, Chen RH, Lin ML (1999) Initiative anatomy of Tungmen debris flow, eastern Taiwan. *Environ Eng Geosci* 5:459–473
- Chen CY, Lin LY, FC Y, Lee CS, Tseng CC, Wang AH, Cheung KW (2007) Improving debris flow monitoring in Taiwan by using high-resolution rainfall products from QPESUMS. *Nat Hazards* 40:447–461
- Chen CW, Saito H, Oguchi T (2015) Rainfall intensity–duration conditions for mass movements in Taiwan. *Progress Earth Planet Sci* 2:1–13
- Chen CW, Chen H, Oguchi T (2016) Distributions of landslides, vegetation, and related sediment yields during typhoon events in northwestern Taiwan. *Geomorphology* 273:1–13
- Chiang SH, Chang KT (2009) Application of radar data to modeling rainfall-induced landslides. *Geomorphology* 103:299–309
- Chou HT, Lee CF, Lo CM (2016) The formation and evolution of a coastal alluvial fan in eastern Taiwan caused by rainfall-induced landslides. *Landslides* (Article in Press)
- Chuang SC, Chen H, Lin GW, Lin CW, Chang CP (2009) Increase in basin sediment yield from landslides in storms following major seismic disturbance. *Eng Geol* 103:59–65
- Crozier MJ (1999) Prediction of rainfall-triggered landslides: a test of the antecedent water status model. *Earth Surf Proc Land* 24:825–833
- Dadson SJ, Hovius N, Chen H, Dade WB, Hsieh ML, Willett SD, JC H, Hornig MJ, Chen MC, Stark CP, Lague D, Lin JC (2003) Links between erosion, runoff variability and seismicity in the Taiwan orogeny. *Nature* 426:648–651
- Dahal R, Hasegawa S (2008) Representative rainfall thresholds for landslides in the Nepal Himalaya. *Geomorphology* 100:429–443
- Dai FC, Lee CF (2002) Landslide characteristics and slope instability modeling using GIS, Lantau Island, Hong Kong. *Geomorphology* 42:213–228
- Fujiwara O, Yanagida M, Shimizu N, Sanga T, Sasaki T (2004) Regional distribution of large landslide landforms in Japan—implication in geology and landform. *Journal of the Japan Landslide Society* 41:335–344 (in Japanese with English abstract)

- Glade T, Crozier M, Smith P (2000) Applying probability determination to refine landslide-triggering rainfall thresholds using an empirical “antecedent daily rainfall model.”. *Pure Appl Geophys* 157:1059–1079
- Gorsevski PV, Brown MK, Panter K, Onasch CM, Simic A, Snyder J (2016) Landslide detection and susceptibility mapping using LiDAR and an artificial neural network approach: a case study in the Cuyahoga Valley National Park, Ohio. *Landslides* 13:467–484
- Guzzetti F, Carrara A, Cardinali M, Reichenbach P (1999) Landslide hazard evaluation: a review of current techniques and their application in a multi-scale study, central Italy. *Geomorphology* 31:181–216
- Guzzetti F, Malamud BD, Turcotte DL, Reichenbach P (2002) Power-law correlations of landslide areas in central Italy. *Earth Planet Sc Lett* 195:169–183
- Guzzetti F, Reichenbach P, Cardinali M, Galli M, Ardizzone F (2005) Probabilistic landslide hazard assessment at the basin scale. *Geomorphology* 72:272–299
- Guzzetti F, Reichenbach P, Ardizzone F, Cardinali M, Galli M (2006) Estimating the quality of landslide susceptibility models. *Geomorphology* 81:166–184
- Guzzetti F, Peruccacci S, Rossi M, Stark C (2007) Rainfall thresholds for the initiation of landslides in central and southern Europe. *Meteorog Atmos Phys* 98:239–267
- Heyerdahl H, Harbitz CB, Domaas U, Sandersen F, Tronstad K, Nowacki F, Engen A, Kjekstad OD, Evoli G, Buezo SG, Diaz MR, Hernandez W (2003) Rainfall induced lahars in volcanic debris in Nicaragua and El Salvador: practical mitigation. In: *Proceedings of International Conference on Fast Slope Movements-Prediction and Prevention for Risk Mitigation, IC-FSM2003, Patron Publ, Naples*, pp 275–282
- Ho CS (1986) A synthesis of the geologic evolution of Taiwan. *Tectonophysics* 125:1–16
- Ishihara Y, Kobatake S (1979) Runoff model for flood forecasting. *Bulletin of Disaster Prevention Research Institute, Kyoto University* 29:27–43
- Jan CD, Lee MH (2004) A debris flow rainfall-based warning model. *J Chin Soil Water Conserv* 35:275–285 (in Chinese with English abstract)
- Janbu N, Bjerrum L, Kjaernsli B (1956) *Stabilitetsberegning for Fyllinger Skjaeringer Ognaturlige Skraninger*. Norwegian Geotechnical Publication 16, Oslo, Norway
- Keefer DK (1984) Landslides caused by earthquakes. *Geol Soc Am Bull* 95:406–421
- Keefer DK, Wilson R, Mark R, Brabb E, Brown W, Ellen S, Harp E, Wieczorek G, Alger C, Zatkun R (1987) Real-time landslide warning during heavy rainfall. *Science* 238:921–925
- Khan YA, Lateh H, Baten MA, Kamil AA (2012) Critical antecedent rainfall conditions for shallow landslides in Chittagong City of Bangladesh. *Environ Earth Sci* 67:97–106
- Kim SK, Hong WP, Kim YM (1991) Prediction of rainfall-triggered landslides in Korea. In: Bell DH (ed) *Landslides*. AA Balkema, Rotterdam, pp. 989–994
- Larsen M, Simon A (1993) A rainfall intensity–duration threshold for landslides in a humid-tropical environment: Puerto Rico. *Geogr Ann A* 75:13–23
- Lee S, Ryu J, Kim I (2007) Landslide susceptibility analysis and its verification using likelihood ratio, logistic regression, and artificial neural network models: case study of Youngin, Korea. *Landslides* 4:327–338
- Li YH (1976) Denudation of Taiwan island since the Pliocene epoch. *Geology* 4:105–107
- Lin Z, Oguchi T, Chen YG, Saito K (2009) Constant-slope alluvial fans and source basins in Taiwan. *Geology* 37:787–790
- Malamud BD, Turcotte DL, Guzzetti F, Reichenbach P (2004a) Landslide inventories and their statistical properties. *Earth Surf Proc Land* 29:687–711
- Malamud BD, Turcotte DL, Guzzetti F, Reichenbach P (2004b) Landslides, earthquakes, and erosion. *Earth Planet Sc Lett* 229:45–59
- Melchiorre C, Matteucci M, Azzoni A, Zanchi A (2008) Artificial neural networks and cluster analysis in landslide susceptibility zonation. *Geomorphology* 94:379–400
- Melillo M, Brunetti MT, Peruccacci S, Gariano SL, Guzzetti F (2015) An algorithm for the objective reconstruction of rainfall events responsible for landslides. *Landslides* 12:311–320
- Morgenstern NR, Price VE (1965) The analysis of the stability of general slip surface. *Geotechnique* 15:79–93
- Okada K, Makihara Y, Shimpo A, Nagata K, Kunitzugu M, Saito K (2001) Soil water index. *Tenki* 47:36–41
- Oku Y, Yoshino J, Takemi T, Ishikawa H (2014) Assessment of heavy rainfall-induced disaster potential based on an ensemble simulation of Typhoon Talas (2011) with controlled track and intensity. *Nat Hazard Earth Sys* 14:2699–2709
- Osanai N, Shimizu T, Kuramoto K, Kojima S, Noro T (2010) Japanese early-warning for debris flows and slope failures using rainfall indices with radial basis function network. *Landslides* 7:325–338
- Pal M, Mather P (2003) An assessment of the effectiveness of decision tree methods for land cover classification. *Remote Sens Environ* 86:554–565
- Paudel U, Oguchi T, Hayakawa Y (2016) Multi-resolution landslide susceptibility analysis using a DEM and random Forest. *Int J Geosci* 7:726
- Rosi A, Peternel T, Jemec-Auflič M, Komac M, Segoni S, Casagli N (2016). Rainfall thresholds for rainfall-induced landslides in Slovenia. *Landslides* (Article in Press)
- Saito H, Matsuyama H (2012) Catastrophic landslide disasters triggered by record-breaking rainfall in Japan: their accurate detection with normalized soil water index. *SOLA* 8:81–84
- Saito H, Nakayama D, Matsuyama H (2009) Comparison of landslide susceptibility based on a decision-tree model and actual landslide occurrence: the Akaishi Mountains, Japan. *Geomorphology* 109:108–121
- Saito H, Nakayama D, Matsuyama H (2010a) Relationship between the initiation of a shallow landslide and rainfall intensity–duration thresholds in Japan. *Geomorphology* 118:167–175
- Saito H, Nakayama D, Matsuyama H (2010b) Two types of rainfall conditions associated with shallow landslide initiation in Japan as revealed by Normalized Soil Water Index. *SOLA* 6:57–60
- Saito H, Korup O, Uchida T, Hayashi S, Oguchi T (2014) Rainfall conditions, typhoon frequency, and contemporary landslide erosion in Japan. *Geology* 42:999–1002
- Saito H, Murakami W, Daimaru H, Oguchi T (2017) Effect of forest clear-cutting on landslide occurrences: analysis of rainfall thresholds at Mt. Ichifusa, Japan. *Geomorphology* 276:1–7
- Sassa K (2005) Landslide disasters triggered by the 2004 Mid-Niigata Prefecture earthquake in Japan. *Landslides* 2:135–142
- Yu SB, Chen HY, Kuo LC (1997) Velocity field of GPS stations in the Taiwan area. *Tectonophysics* 274:41–59
- Schneevoigt N, van der Linden S, Thamm H, Schrott L (2008) Detecting Alpine landforms from remotely sensed imagery. A pilot study in the Bavarian Alps. *Geomorphology* 93:104–119
- Segoni S, Battistini A, Rossi G, Rosi A, Lagomarsino D, Catani F, Moretti S, Casagli N (2015a) Technical note: an operational landslide early warning system at regional scale based on space–time-variable rainfall thresholds. *Nat Hazards Earth Syst Sci* 15:853–861
- Segoni S, Lagomarsino D, Fanti R, Moretti S, Casagli N (2015b) Integration of rainfall thresholds and susceptibility maps in the Emilia Romagna (Italy) regional-scale landslide warning system. *Landslides* 12:773–785
- Shieh SL (2000) User’s guide for typhoon forecasting in the Taiwan area (VIII). Central Weather Bureau, Taipei
- Spencer E (1967) A method of analysis of the stability of embankments assuming parallel inter-slice forces. *Geotechnique* 12:11–26
- Sugawara M, Ozaki E, Watanabe I, Katsuyama Y (1974) Tank model and its application to Bird Creek, Wollombi Brook, Bikin River, Kitsu River, Sanaga River and Nam Mune. *Res Note Natl Res Center Disaster Prev* 11:1–64
- Tao T, Chocat B, Liu S, Xin K (2009) Uncertainty analysis of interpolation methods in rainfall spatial distribution—a case of small catchment in Lyon. *J Environ Prot* 1:50–58
- Teng LS (1990) Geotectonic evolution of late Cenozoic arc-continent collision in Taiwan. *Tectonophysics* 183:57–76
- Tiranti D, Rabuffetti D (2010) Estimation of rainfall thresholds triggering shallow landslides for an operational warning system implementation. *Landslides* 7:471–481
- Tiranti D, Rabuffetti D, Salandin A, Tararbra M (2013) Development of a new translational and rotational slides prediction model in Langhe hills (north-western Italy) and its application to the 2011 March landslide event. *Landslides* 10:121–138
- Tsangaratos P, Ilia I (2016) Landslide susceptibility mapping using a modified decision tree classifier in the Xanthi Prefecture, Greece. *Landslides* 13:305–320
- Vessia G, Parise M, Brunetti MT, Peruccacci S, Rossi M, Vennari C, Guzzetti F (2014) Automated reconstruction of rainfall events responsible for shallow landslides. *Nat Hazards Earth Syst Sci* 14:2399–2408
- Wang B, Ho L (2002) Rainy season of the Asian-Pacific summer monsoon. *J Clim* 15:386–398
- Wieczorek GF, Glade T (2005) Climatic factors influencing occurrence of debris flows. In: Jakob M, Hunger O (eds) *Debris-flow hazards and related phenomena*. Springer-Verlag, Berlin, pp. 325–362
- Willett SD, Fisher D, Fuller C, Yeh EC, Lu CY (2003) Erosion rates and orogenic wedge kinematics in Taiwan inferred from apatite fission track thermochronometry. *Geology* 31:945–948
- Wu CC, Kuo YH (1999) Typhoons affecting Taiwan: current understanding and future challenges. *B Am Meteorol Soc* 80:67–80
- Xu M, Watanachaturaporn P, Varshney P, Arora M (2005) Decision tree regression for soft classification of remote sensing data. *Remote Sens Environ* 97:322–336

C. Chen (✉) · H. Saito · T. Oguchi

Center for Spatial Information Science,  
University of Tokyo,  
5-1-5 Kashiwanoha, Kashiwa, Chiba 277-8568, Japan  
e-mail: kevin4919@gmail.com

C. Chen

National Science and Technology Center for Disaster Reduction,  
No. 200, Sec. 3, Beixin Road, Xindin District, New Taipei City, Taiwan

H. Saito

College of Economics,  
Kanto Gakuin University,  
1-5-1 Mutsuura-higashi, Yokohama, Kanagawa 236-8501, Japan